



## OPEN

SUBJECT AREAS:  
BATTERIES  
ELECTROCHEMISTRY  
NANOPARTICLESReceived  
10 December 2013Accepted  
27 January 2014Published  
10 February 2014Correspondence and  
requests for materials  
should be addressed to  
J.K. (jaekook@  
chonnam.ac.kr)\* These authors  
contributed equally to  
this work.Pyro-synthesis of a high rate nano- $\text{Li}_3\text{V}_2(\text{PO}_4)_3/\text{C}$  cathode with mixed morphology for advanced Li-ion batteriesJungwon Kang<sup>1\*</sup>, Vinod Mathew<sup>1\*</sup>, Jihyeon Gim<sup>1</sup>, Sungjin Kim<sup>1</sup>, Jinju Song<sup>1</sup>, Won Bin Im<sup>1</sup>, Junhee Han<sup>2</sup>, Jeong Yong Lee<sup>2,3</sup> & Jaekook Kim<sup>1</sup><sup>1</sup>Department of Materials Science and Engineering, Chonnam National University, 300 Yongbong-dong, Bukgu, Gwangju 500-757, South Korea, <sup>2</sup>Department of Materials Science and Engineering, KAIST, 335 Gwahangno, Yuseung-gu, Daejeon 305-701, South Korea, <sup>3</sup>Center for Nanomaterials and chemical reactions, Institute for Basic Science, Daejeon 305-701, South Korea.

A monoclinic  $\text{Li}_3\text{V}_2(\text{PO}_4)_3/\text{C}$  (LVP/C) cathode for lithium battery applications was synthesized by a polyol-assisted pyro-synthesis. The polyol in the present synthesis acts not only as a solvent, reducing agent and a carbon source but also as a low-cost fuel that facilitates a combustion process combined with the release of ultrahigh exothermic energy useful for nucleation process. Subsequent annealing of the amorphous particles at 800 °C for 5 h is sufficient to produce highly crystalline LVP/C nanoparticles. A combined analysis of X-ray diffraction (XRD) and neutron powder diffraction (NPD) patterns was used to determine the unit cell parameters of the prepared LVP/C. Electron microscopic studies revealed rod-type particles of length ranging from nanometer to micrometers dispersed among spherical particles with average particle-sizes in the range of 20–30 nm. When tested for Li-insertion properties in the potential windows of 3–4.3 and 3–4.8 V, the LVP/C cathode demonstrated initial discharge capacities of 131 and 196 mAh/g (~100% theoretical capacities) at 0.15 and 0.1 C current densities respectively with impressive capacity retentions for 50 cycles. Interestingly, the LVP/C cathode delivered average specific capacities of 125 and 90 mAh/g at current densities of 9.6 C and 15 C respectively within the lower potential window.

Rechargeable lithium ion batteries (LIBs) are considered as one of the most promising power sources for electric vehicle (EV) and hybrid electric vehicle (HEV) applications<sup>1</sup>. The present state of affairs in the emerging market of Li-ion batteries indicate that any Li-battery cathode requires to satisfy the demands of fast charging capability, high energy density, long shelf-life and safety issues. Bearing this in mind, intense efforts are on to identify phosphate-based cathodes due to the strongly covalent  $(\text{PO}_4)^{3-}$  units that provide greater structural stability than commercial  $\text{LiCoO}_2$  hosts even under deep charging conditions and elevated temperatures<sup>2–9</sup>. Among the known phosphates, monoclinic  $\text{Li}_3\text{V}_2(\text{PO}_4)_3$  (LVP) is a promising LIB cathode due to its high operating voltage (~4 V) and ability to deliver a maximum theoretical capacity of 197 mAh g<sup>-1</sup> as 3Li<sup>+</sup> ions are extracted/inserted per unit in the voltage range 3.0–4.8 V. However, monoclinic LVP suffers from low electrical conductivity (~2.4 × 10<sup>-8</sup> S cm<sup>-1</sup>) and hence the complete utilization of its theoretical capacity coupled with high rate performances becomes intricate. A majority of the strategies to overcome this obstacle is focused on producing particles with electrically conductive coatings or composites<sup>5,10–13</sup> and reducing particle sizes<sup>14,15</sup>. Given the fact that reversible insertion of all three Li atoms that occupy distinct crystallographic positions in monoclinic LVP phase is feasible under slow or even fast charge/discharge rates, literatures on carbon coatings and developing composites of micro-sized LVP are available<sup>13,16–21</sup>. Nevertheless, only a few studies on the solid state and sol-gel syntheses of nanostructured LVP are reported<sup>5,11,15</sup>. One of the difficulties to prepare nano-sized LVP is probably due to the high crystallization energies which may not only lead to unavoidable particle growth at elevated temperatures but also make carbon coating or composite formation complicated<sup>17–21</sup>. Meanwhile, polyol approaches are advantageous for the preparation of electrode materials at considerably moderate temperatures. Moreover, poly alcohols or polyols such as ethylene glycol and di/tri/tetra ethylene glycol can play multi-roles of a solvent, a reducing agent and a carbon source<sup>22–25</sup>. Further, the importance of combustion based approaches to synthesize LVP electrodes have also been highlighted recently<sup>26,27</sup>. Hence, it remains essential to develop synthetic routes wherein particle crystallization and limiting particle growth are facilitated simultaneously in order to arrive at optimized carbon coated/composite LVP nanoparticles with high power capabilities.



Herein, we report a pyro-synthesis performed in a polyol medium that acts as a solvent, a conductive carbon source and a reducing agent to maintain lower vanadium oxidation states of V (III) and facilitate the formation of LVP. Further, the polyol acts a low-cost fuel, which on combustion yields carbonized structures that may aid in carbon coating and tend to restrict excessive particle growth. Our previous report on a rhombohedra  $\text{Na}_3\text{V}_2(\text{PO}_4)_3/\text{C}$  cathode produced by this pyro-technique revealed the presence of micro and nano-sized particles. The prepared NVP/C cathode clearly demonstrated the possibility of reversible insertion of 4  $\text{Na}^+$  ions within the potential window of 3.8 – 1.5 V vs  $\text{Na}/\text{Na}^{+22}$ . Hence, the pyro-synthesis was employed in the present study to produce an LVP/C cathode and assess its insertion capabilities within different potential windows at various charge/discharge rates. The as-prepared carbon-saturated  $\text{Li}_3\text{V}_2(\text{PO}_4)_3$  possesses amorphous characteristics and require post-heat treatment for complete particle crystallization. However, the as-prepared amorphous LVP/C requires apparently shorter sintering reaction times of approximately 5 h to produce carbon-coated particles that does not display excessive growth. Moreover, the saturated carbon on LVP particles appears to prevent the particle growth even at high sintering temperatures of  $\sim 800^\circ\text{C}$ . Although particle growth, to a certain extent, is inevitable at elevated temperatures, the morphology of the prepared sample indicates the presence of spherical and rod-shaped particles with surface carbon coatings. The conductive coating may not only tend to prevent excessive particle growth at high temperatures but also enhance the electrical conductivity of the prepared LVP. In addition, the existence of a carbon network that may improve the electrical connectivity between the particles is also revealed. All these factors appear to significantly influence the overall electrochemical performance of the prepared LVP/C cathode that demonstrated decent reversible insertion of  $2/3 \text{Li}^+$  ions even under high current densities.

## Results and discussion

The polyol assisted pyro-synthesis to obtain  $\text{Li}_3\text{V}_2(\text{PO}_4)_3/\text{C}$  is a straightforward approach and is clearly illustrated in Figure 1. The first stage is represented by the complete dissolution of the starting precursors in the polyol solution. The subsequent stage involves the ignition of the homogenous solution with a torch which ultimately results in the rapid precipitation of nanoparticles. In fact, the polyol, ethylene glycol acts as a low-cost fuel that induces a flame and thereby releases ultrahigh exothermic energy which is usefully exploited for precursor decomposition and subsequent nucleation of nanoparticles. The entire reaction proceeds as a continuous process and is completed in just a few seconds. In addition, the presence of phosphoric acid ( $\text{H}_3\text{PO}_4$ ) accelerates the carbonization of the polyol to yield carbocations and carbon-carbon double bonds at high temperatures<sup>28</sup>. The resulting carbonized structures may act as physical barriers to prevent particle growth at elevated reaction temperatures. Further, the generation of high energy coupled with the short

reaction time facilitates rapid nucleation and tend to suppress grain growth. The hydrocarbon containing polyol serve as a carbon source and the reducing environment offered by the polyol ensures that vanadium is maintained at the lower V(III) state. The as-prepared sample obtained after the pyro-synthetic reaction in Figure 1 corresponds to the carbon-saturated amorphous  $\text{Li}_3\text{V}_2(\text{PO}_4)_3$  particles. The post heat-treatment at  $800^\circ\text{C}$  in argon atmosphere for a short sintering time of 5 h is sufficient to produce highly crystalline particles. Although the elevated heat treatment tends to make particle growth inevitable, the carbonized structures formed from polyol combustion may prevent excessive particle growth. Further, the presence of a carbon network that may act as electrical conduits between the particles may tend to improve the electrochemical properties at even high charge/discharge rates.

The crystal structure of LVP/C was elucidated by a combined analysis of the Rietveld refinement performed on the X-ray and neutron diffraction data of the prepared sample. In general, the common problem of detecting lighter atoms (Li) in the presence of heavy transition atoms (V) with many electrons using X-ray maybe overcome by using neutron diffraction which can produce scattered rays of proportional intensities from all atoms irrespective of being light or heavy. Therefore, a combined Rietveld refinement analysis on the X-ray and neutron diffraction data was performed to estimate the structural parameters of LVP and the results are summarized in Table 1 and Table S1 (see Supporting Information). The fitted patterns obtained from the X-ray and neutron diffraction studies are shown in Figures 2a and b respectively. The space group for  $\text{Li}_3\text{V}_2(\text{PO}_4)_3$  was determined as  $P2_1/n$  and, as anticipated, all the constituent atoms including the three lithium atoms, in the monoclinic unit cell are distributed over distinct co-ordinates at the crystallographic  $4e$  site (Fig. 2c). The refined lattice parameter values are slightly lower and the lattice volume of the monoclinic unit cell is significantly lower in the present  $\text{Li}_3\text{V}_2(\text{PO}_4)_3/\text{C}$  than those reported<sup>5,11,20,29–34</sup>. In general, the reported lattice volume for LVP/C is relatively higher than that for pure LVP. However, in the present study, the estimated lattice volume of  $886.9 \text{ \AA}^3$  for the monoclinic unit cell is the lowest so far among the reported values for LVP and LVP/C samples. According to Liu et. al, the estimated lattice-volume may depend on the presence of carbon or graphene in the sample<sup>30</sup>. The fractional coordinates of the elements are in close agreement with those reported for monoclinic  $\text{Li}_3\text{V}_2(\text{PO}_4)_3$ . Moreover, it is well known that the atomic positions of Li are critical to influence the electrochemical performance of  $\text{Li}_3\text{V}_2(\text{PO}_4)_3$ <sup>30</sup>. The three distinct Li sites in the monoclinic lattice at room temperature consist of one four-fold co-ordination (Li1) and two five-fold co-ordination (Li2 and Li3) sites. The refined isotropic thermal data indicate that the values for the Li atoms situated at two locations (Li1 and Li2) are far higher than that of the third lithium site (Li3) (see Table S1, Supporting Information). This observation clearly indicates that the Li1 and Li2 sites predominantly contribute to ionic conduction.

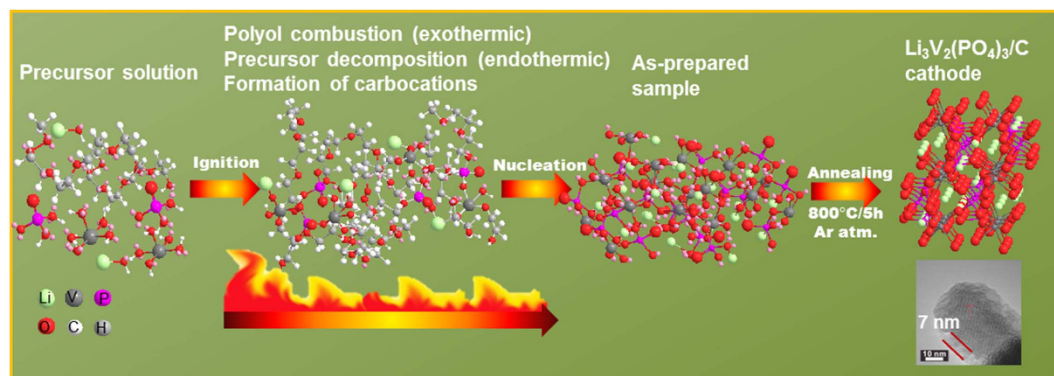


**Figure 1** | Schematic diagram of the pyro-synthesis to obtain LVP/C cathode.



**Table 1** | Rietveld refinement and crystal data  $\text{Li}_3\text{V}_2(\text{PO}_4)_3$  by neutron and X-ray diffraction. The numbers in parentheses are the estimated standard deviations of the last significant figure

Formula	$\text{Li}_3\text{V}_2(\text{PO}_4)_3$	
Radiation type	$\text{CuK}\alpha$	Neutron
$2\theta$ range (degree)	10–140	15–160
T/K	295	295
Symmetry	Monoclinic	
Space group	$\text{P}2_1/\text{n}$	
a/Å	8.571(5)	
b/Å	8.615(5)	
c/Å	12.010(6)	
$\beta$ (degree)	90.15(8)	
Volume/Å <sup>3</sup>	886.9(1)	
Z	4	
$R_p$	3.40%	
$R_{wp}$	4.47%	
$\chi^2$	1.82	

Although the Li2 and Li3 sites in the present  $\text{Li}_3\text{V}_2(\text{PO}_4)_3$  are swapped in comparison to that studied by Patoux et. al, the result is contrary to the finding by the latter that the five-fold co-ordination sites (Li2, Li3) are mainly involved in ionic conduction<sup>20</sup>. The bond lengths and bond angles specific to Li sites were calculated using VESTA software and are listed in Table S2 (see Supporting Information). The Li-O bond lengths at the tetrahedral Li1 site vary between 1.87 and 2.04 Å. On the other hand, the longest Li-O bond lengths at the pseudo-tetrahedral Li2 and Li3 sites are calculated to be 2.61 and 2.33 Å respectively. The V-O bond distances for the two slightly distorted  $\text{VO}_6$  octahedral units representing two distinctive vanadium sites V1 and V2 are estimated to lie in the ranges of 1.82–2.17 Å and 1.88–2.12 Å respectively (Table S2). The bond-valence sum values for the two octahedral sites of vanadium, namely V1 and V2, were determined to be 3.2 and 3.5 respectively. The calculated values thus indicate that the oxidation states of vanadium are close to +3. The average bond lengths of the  $\text{PO}_4$  tetrahedral units vary between 1.54 and 1.61 Å (Table S2, Supporting Information). Furthermore, the low values of reliability ( $\chi^2 < 2$ ) and weighted ( $R_p, R_{wp} < 5\%$ ) factors indicate the consistency of the combined refinement analysis. The ICP analysis also confirmed the molar stoichiometric composition of the prepared  $\text{Li}_3\text{V}_2(\text{PO}_4)_3$  (Table S3,

Supporting Information). Electron microscopic images of the prepared LVP/C were recorded to obtain further information on the particle size/morphology and carbon existence. Figure 3a shows the low-magnification field emission scanning electron microscopy (FE-SEM) image of LVP/C that appears to reveal rod-type particles dispersed among a major portion of apparently smaller particles with spherical morphologies. The rod-shaped particles are observed to range from a few hundred nanometers to micrometers (Figure 3a). This observation implies that particle growth remains unavoidable due to sintering of the as-prepared sample at elevated temperatures. Further, the average particle-sizes of the spherical particles are observed to be in the range of 20–30 nm. In addition, the high magnification SEM image in Figure 3a inset appears to reveal some aggregation between particles. It is highly probable that the short sintering time (~5 h) may be insufficient to cause excessive particle growth even at elevated temperatures (~800°C). The as-prepared LVP which shows amorphous characteristics or consists of loosely bound functional groups at the atomic scale may undergo phase transition to highly crystalline nanoparticles even under very short sintering times. Furthermore, the carbonized structures formed from polyol combustion may not only contribute to limiting particle growth but also facilitate the maintenance of vanadium in the lower V (III) oxidation state. The Transmission electron microscopy (TEM) images of LVP/C under low and high magnification are shown in Figure 3(b–f). The contrast observed in the image of Figure 3b clearly appears to distinguish between the carbon-coated particles and the carbon network present in the sample. The relatively darker locations appear to indicate the presence of carbon-coated LVP particles whereas the brighter image seems to display a network-type structure of probably carbon. Fig. 3c shows the tip of a single rod-type particle and the corresponding high magnification image is presented in Figure 3d. The highly magnified picture reveals that the lattice fringe value of 3.03 Å is distinguishable in addition to identifying a carbon-coating of 7 nm thickness along the particle boundary. The Fourier transform (FFT) image of the corresponding area is also shown in the inset of Figure 3d. On the other hand, Figure 3e shows a LVP particle with spherical-type morphology. The corresponding high magnification image, displayed in Figure 3f, directly visualizes the lattice fringe in the spherical particle. Further, the FFT image of the portion under study is shown in Figure 3f inset and confirms the crystalline characteristics of the prepared LVP. It is possible that the mixed morphologies of spherical

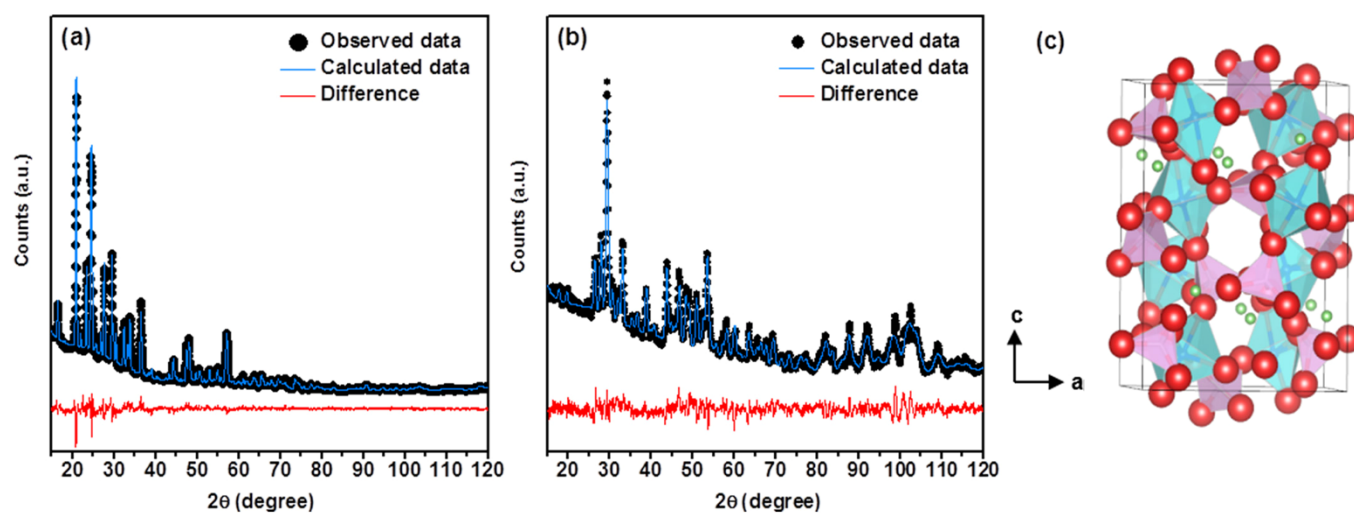


**Figure 2** | Rietveld refinement patterns of  $\text{Li}_3\text{V}_2(\text{PO}_4)_3$  using (a) X-ray powder and (b) neutron diffraction data. Black solid circles represent the observed intensities, and the blue solid line defines calculated ones. The difference (obs. – cal.) plot is shown beneath. (c) The monoclinic LVP lattice derived from the VESTA software using the refined XRD and NPD data. The octahedral ( $\text{VO}_6$ ) and ( $\text{PO}_4$ ) tetrahedral units in addition to Li sites are clearly visible.

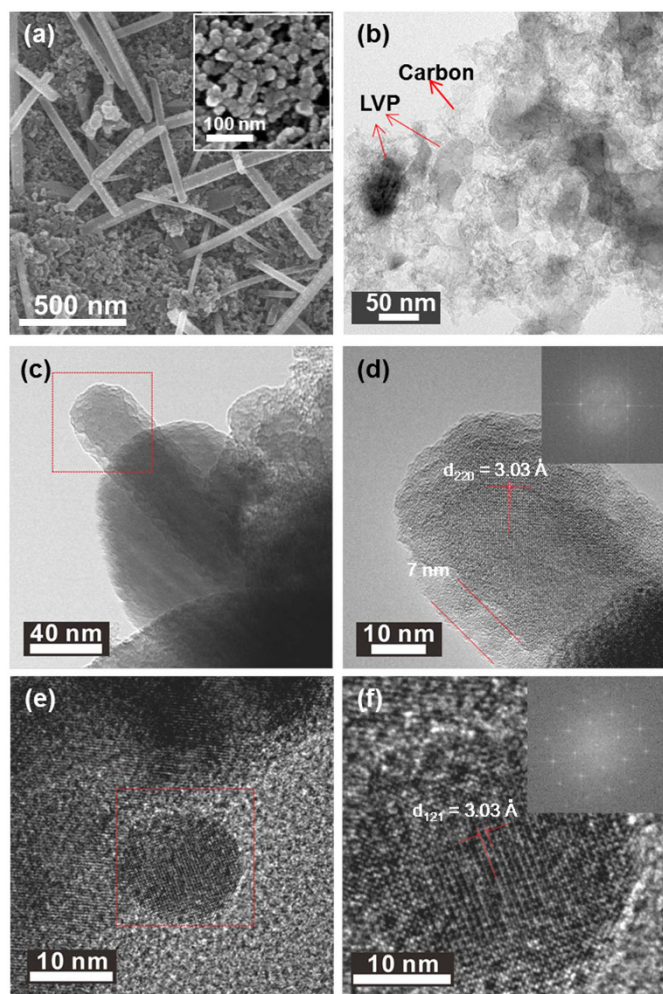


**Figure 3** | (a) SEM image of  $\text{Li}_3\text{V}_2(\text{PO}_4)_3/\text{C}$  obtained by pyro-synthesis and high magnification SEM in inset. (b) TEM image of LVP/C showing LVP particles and carbon network. (c) TEM image showing the tip of a rod-type particle of LVP. (d) HRTEM image of a single rod-type particle with lattice fringes and the inset shows the FFT image. (e) HRTEM image of a spherical particle with (f) the lattice fringe identified and FFT image in the inset.

and rod-type particles may promote intimate particle connectivity and thereby influence electrical properties and hence electrochemical performance<sup>35</sup>. The Energy Dispersive X-ray (EDX) elemental mapping studies were performed to further confirm the presence of carbon in the sample. Figure 4 shows the dark field (DF) STEM image and the corresponding elemental mapping images of C, V and P. The images reveal that carbon is well-dispersed among the sample and is similar to that procured for the counterpart elements of V and P. The observation, therefore, appears to indicate the presence of surface carbon coatings and indirectly suggests the presence of a carbon-network as well among the LVP particles. The elemental analysis confirmed that the carbon content on the prepared LVP/C was 6.87%. The estimated value appears to be sufficient enough to facilitate the carbon layer and network formation<sup>12,36,37</sup>. The decent dispersion of the respective elements in the sample implies that no phase separations in the nanometer scale occurred during the formation of LVP/C particles. Further, the Brunauer-Emmett-Teller (BET) analysis aided in estimating the surface area of the sample to be  $124.15 \text{ m}^2\text{g}^{-1}$ .

It is anticipated that the combined factors of carbon painting on LVP and the presence of a carbon-network facilitates the enhancement of electrical conductivity in the prepared phosphate cathode. Figure 5 presents the electrochemical performances of the LVP/C

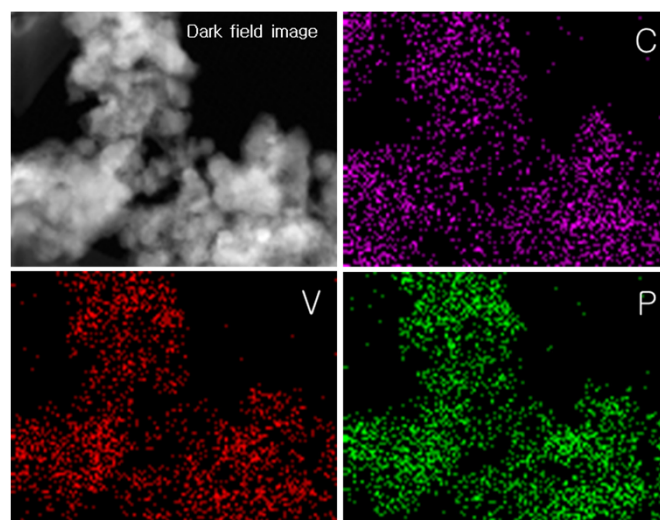


**Figure 4** | Elemental mapping images of LVP/C prepared by pyro-synthetic reaction; dark-field (DF) image and the elemental distributions

electrode vs  $\text{Li}^0/\text{Li}^+$ . The LVP/C electrode was cycled under two potential ranges of 3–4.3 and 3–4.8 V at a current density of  $0.1 \text{ mA cm}^{-2}$ . Figure 5a presents the initial voltage curve of the LVP/C electrode at 0.15 C in the voltage range of 3.0 ~ 4.3 V. The charge curve reveals two lower plateaus at 3.6 and 3.68 V that corresponds to the two-step extraction of one Li from  $\text{Li}_3\text{V}_2(\text{PO}_4)_3$  and therefore indicate the presence of mixed V(III)/V(IV) oxidation states. The charge plateau at 4.08 V represents a one-step extraction of the second Li from the monoclinic structure and hence the complete oxidation of V (III) to V (IV) state. On the other hand, the discharge curve reveals a potential plateau at 4.04 V that corresponds to re-insertion of one Li into the monoclinic  $\text{LiV}_2(\text{PO}_4)_3$  structure. The discharge plateaus that occur at two potentials namely, 3.64 and 3.55 V correspond to the re-insertion of the second Li into the monoclinic host. On completion of the discharge cycle, the complete reduction from V (IV) to V (III) state in the monoclinic host is ensured. The delivered initial specific discharge capacity is  $131 \text{ mAh/g}$ , which corresponds to almost 100% theoretical capacity ( $\sim 132 \text{ mAh/g}$ ) utilization. The slightly higher value of first charge capacity ( $\sim 143 \text{ mAh/g}$ ) may be considered as a common problem of initial electrochemical activation of active materials. Average discharge capacities of about  $131 \text{ mAh/g}$  (Fig. 5a inset) are consistently maintained with almost 100% Coulombic efficiencies at a current density of 0.15 C (10 mA/g) for 50 electrochemical cycles. Hence, the 100% utilization of theoretical capacity by the prepared LVP/C cathode corresponds to the successful reversible insertion of 2 Li per formula. Further, the differential capacity ( $dQ/dV$ ) plot displayed in Figure 5c clearly reveals that Li-insertion is reversible within the potential window of 3–4.3 V.

The electrochemical response of the prepared LVP/C cathode under a voltage window of 3.0 – 4.8 V is displayed in Figure 5b. The initial voltage curves reveal that a discharge capacity of  $196 \text{ mAh/g}$ , which corresponds to almost 100% of theoretical capacity ( $\sim 197 \text{ mAh/g}$ ), is achieved under a current density of 0.1 C (20 mA/g). The apparently higher discharge capacity delivered by the LVP/C cathode within the wider potential window corresponds to the insertion/extraction of 3Li per  $\text{Li}_3\text{V}_2(\text{PO}_4)_3$ . Precisely, the sloping charge profile in the potential range of 4.5–4.8 V may be assigned to the kinetically difficult extraction process of the third Li and the formation of  $\text{V}_2(\text{PO}_4)_3$ . However, the disorder caused by the vanadium charge ordering in this fully de-lithiated phase contributes to the solid solution phase behaviour observed during the corresponding discharge cycle<sup>29</sup>. The differential capacity ( $dQ/dV$ ) plots in Figure 5d reveal a broad but not so intense peak around

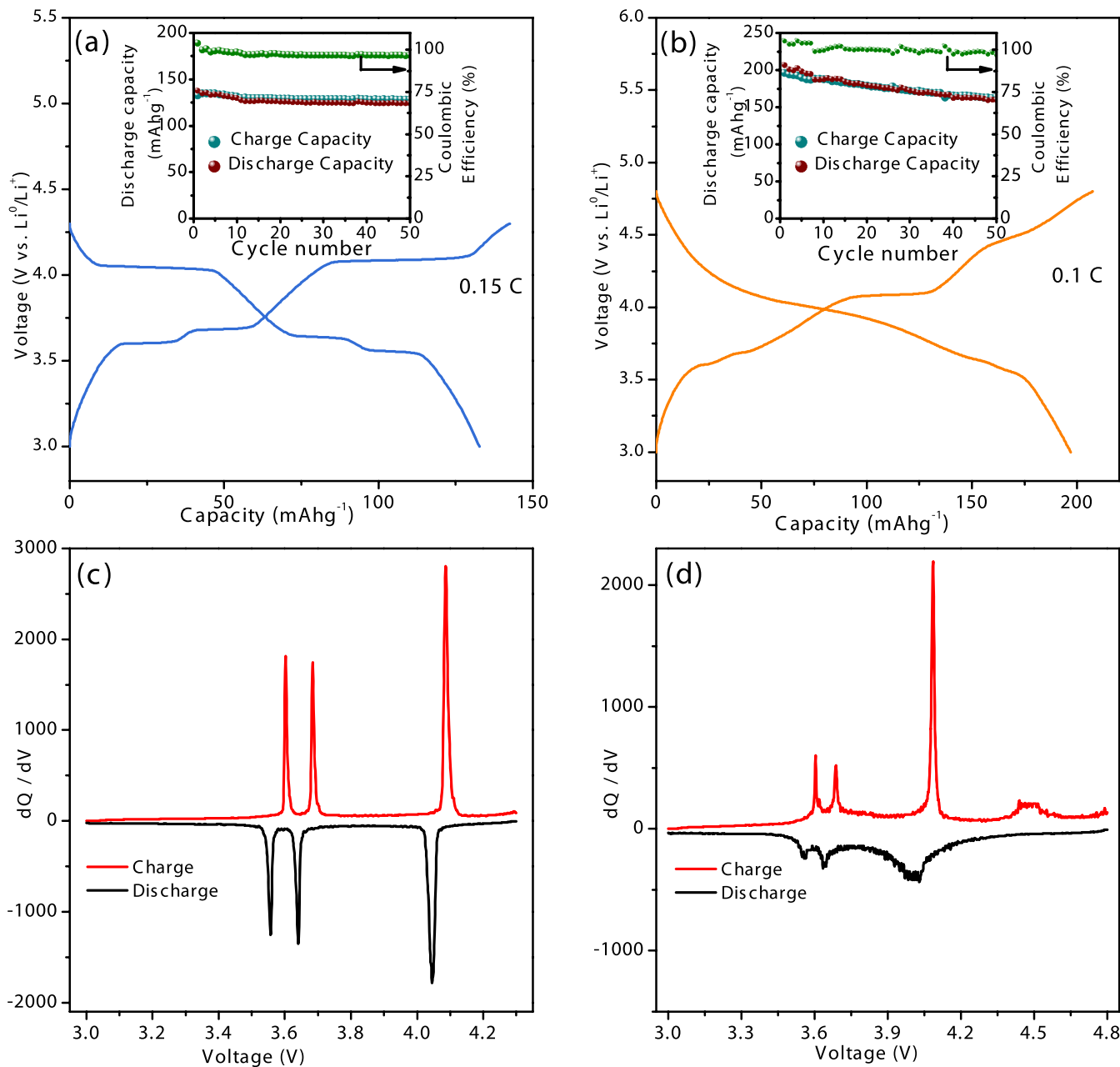


**Figure 5** | Initial discharge profile of  $\text{Li}_3\text{V}_2(\text{PO}_4)_3/\text{C}$  cathode obtained by pyro synthesis within the cycling potential range of (a) 3–4.3 and (b) 3–4.8 V with corresponding cyclabilities and Coulombic efficiencies in the insets. The differential capacity ( $dQ/dV$ ) plots for the half-cells tested under (c) 3–4.3 V and (d) 3–4.8 V conditions.

4.5 V that corresponds to the extraction of the 3<sup>rd</sup> Li during charging. On the other hand, the broad nature of the peak around 4.0 V during discharge may indicate the formation of a  $\text{Li}_x\text{V}_2(\text{PO}_4)_3$  solid solution, as revealed by the sloping discharge profile of the test cell cycled between 3–4.8 V. Although Coulombic efficiencies are maintained in proximities to 100% under extended cycling (Figure 5b inset), the cycle performance of the LVP/C cathode indicates that initial discharge capacity is decreased to 85% after 50 cycles. To procure more information on the capacity fading in the present LVP/C cathode, in-situ XRD measurements were performed on a specially designed half cell (see details in Methods section). The spectro-electrochemical cell was put under galvanostatic test within the potential of 3–4.3 V for the initial cycle. The galvanostatic measurement during the second cycle was performed within the wider potential domain of 3–4.8 V. The electrochemical curves obtained for the initial cycle (3–4.3 V) and the second cycle (3–4.8 V) are provided in Figures 6a and 6b

respectively. The vertical bars that indicate the specific locations at which the XRD scans were initiated are numbered sequentially. The initial ten XRD scans were initiated at progressive state of charges (SOCs) during initial charging until 4.3 V whereas the following eleven scans (from 11 to 21) were recorded at different state of discharges (SODs) during subsequent discharging until 3 V. The in-situ XRD patterns procured at different SOC and SOD during first charging and discharging are plotted against the scan numbers in Figures 6c and 6e respectively. On the other hand, the scan numbers 22 to 31 and 32 to 42 correspond to the different SOC and SOD, respectively, in the second cycle (Figure 6b). The in-situ XRD patterns recorded at various SOC and SOD of the second cycle are presented against their scan numbers in Figures 6c and 6e respectively. The major diffraction lines of the LVP have been marked in Figure 6(c–f) in order to identify the changes in the peak positions during electrochemical cycling. On comparing the XRD patterns

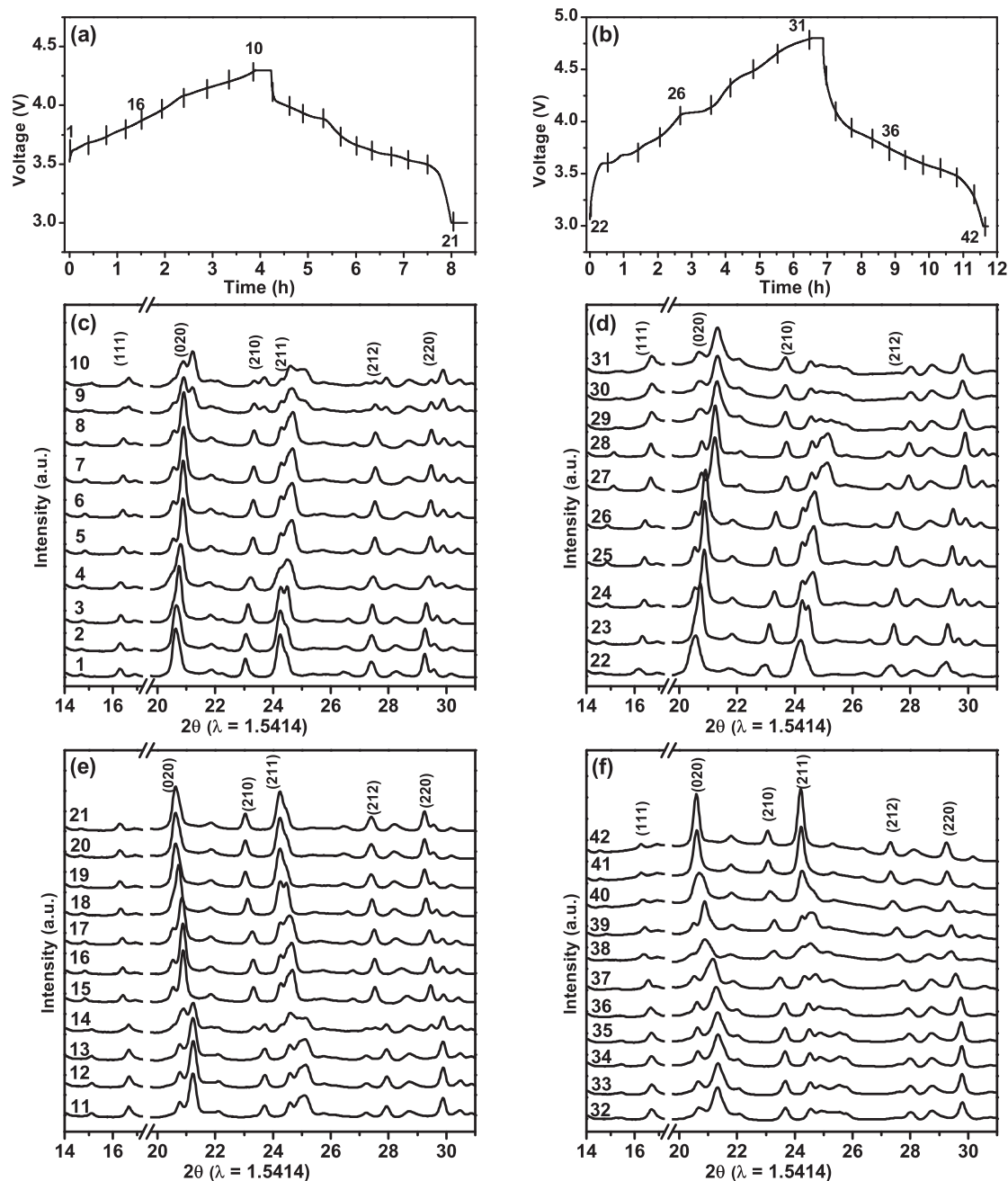


**Figure 6** | The electrochemical profiles of the spectro-electrochemical test cell (a) for the first cycle within the potential window 3–4.3 V and (b) for the second cycle within the potential window 3–4.8 V. The corresponding in-situ XRD patterns recorded during (c) first charging until 4.3 V, (d) second charging until 4.8 V, (e) first discharging until 3 V and (f) second discharging until 3 V.

obtained before and after the first electrochemical cycling (scan numbers 1 and 21) within the potential region of 3–4.3 V, no significant variations in the diffraction peak positions are observed. A similar trend in the positions of the major diffraction peaks is observed before and after the completion of the second cycling within the potential domain of 3–4.8 V. This finding indeed supports the conclusion of a recent investigation that the structural integrity of the LVP/C cathode is maintained in spite of the two-phase reaction mechanism and the large volume changes<sup>38</sup>. Therefore, the present results clearly suggest that the capacity fading observed when the LVP/C cathode is cycled to cut-off potentials of 4.8 V may be related to the kinetic problems or the high resistance offered towards the de-intercalation of the final  $\text{Li}^+$  ion  $[\text{Li}_{3-x}\text{V}_2(\text{PO}_4)_3, (x \geq 2)]$ <sup>29</sup>. Precisely, the fully de-lithiated phase of  $\text{V}_2(\text{PO}_4)_3$  that exhibits some disorder-

ing undergoes a lithium-site/electron ordering or a disorder-to-order transition during the first lithium insertion that ultimately increases the unit cell size of  $\text{LiV}_2(\text{PO}_4)_3$ . The small increase in the unit cell dimensions of  $\text{LiV}_2(\text{PO}_4)_3$  formed during discharging affects the kinetics of the electrochemical reaction and leads to the detrimental effect on the cycle performance of the LVP/C cathode when cycled until high cut-off potentials of 4.8 V.

In order to assess the rate capabilities, the C-rate performances of the prepared LVP/C cathode under the two different potential windows corresponding to the reversible intercalation of 2 and 3 Li ions per formula are displayed in Figure 7(a–d). Namely, a discharge capacity in the proximity of 130 mAh/g corresponding to 2 Li per formula is realized even at a relatively high current density of 640 mA/g (4.8 C). At a current density of 1280 mA/g (9.6 C), an

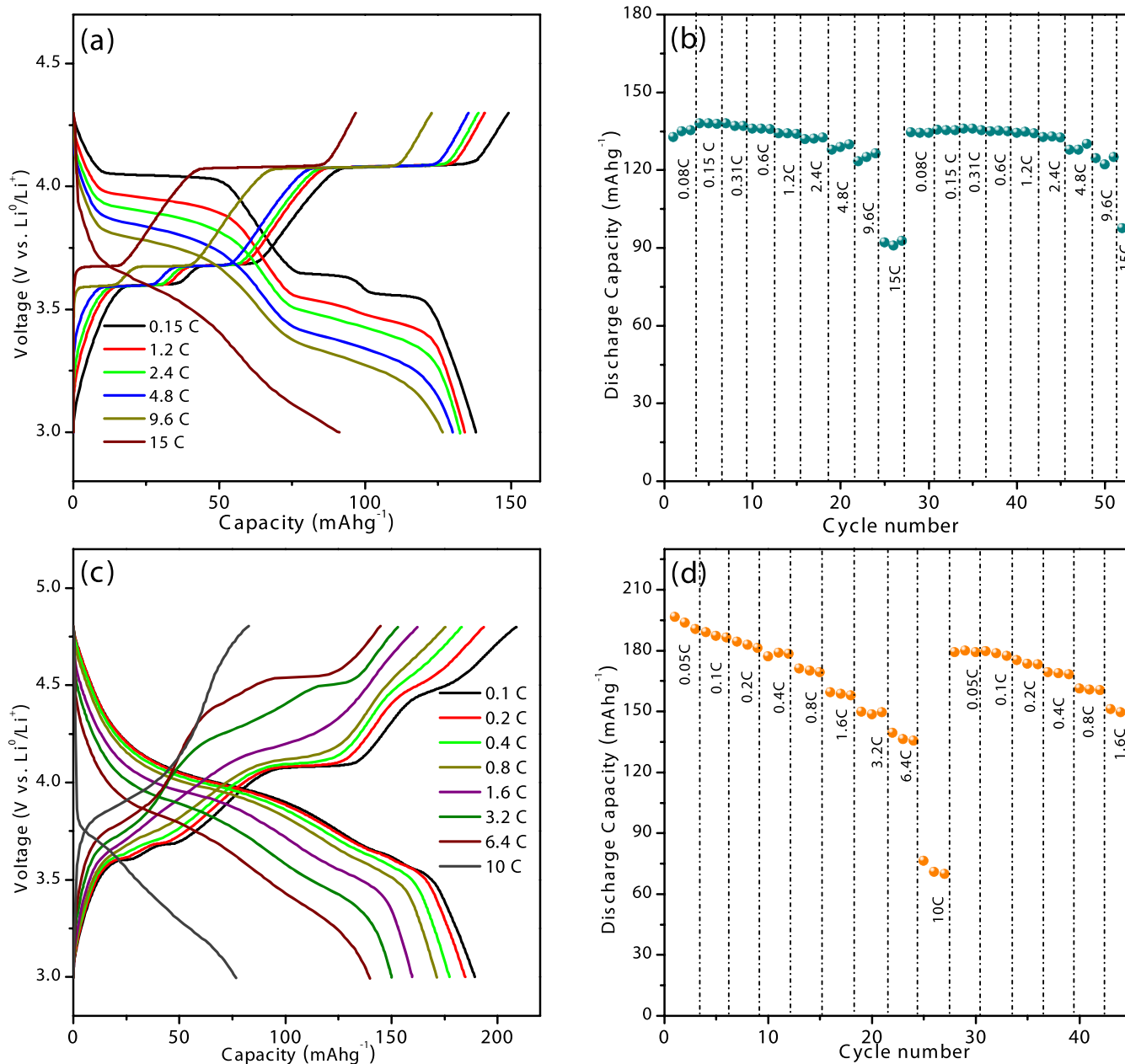


**Figure 7** | (a) The voltage profiles of the LVP/C cathode at different current densities when cycled under a potential range of 3–4.3 V and (b) the C-rate performance values. (c) The electrochemical response of the LVP/C cathode at different current densities under the wider potential range of 3–4.8 V and (d) the corresponding C-rate performance values.

average discharge capacity of 125  $\text{mAh/g}$  corresponding to 95% theoretical value is maintained. It is worth noting that a remarkable average capacity of about 90  $\text{mAh/g}$ , corresponding to 68% of theoretical capacity is achieved at rates as high as a current density of 2000  $\text{mA/g}$  (15 C) (Figure 7 a,b). The first set of current rates applied to the test cell beginning from 0.05 C until 15 C completes after the 27<sup>th</sup> cycle. From the 28<sup>th</sup> cycle, the same set of current densities beginning from 0.05 C is repeated sequentially. It is clearly seen that as the applied current rate is progressively increased from 0.05 to 0.3 C, average capacities of 132  $\text{mAh/g}$  that correspond to 100% theoretical capacity utilization is still delivered by the LVP/C cathode (Figure 7b). In fact, reports on LVP/C cathodes with different morphologies demonstrating capacities in proximities to 100  $\text{mAh/g}$  at current densities beyond 10 C rates are available<sup>13,15,23</sup>. An LVP/Graphene nanocomposite prepared by a sol-gel method demonstrated consistent capacities of 118 and 109  $\text{mAh/g}$  at 5 and 20 C

rates respectively<sup>11</sup>. The specific capacities registered by the present LVP/C cathode are indeed comparable to the reported values. Despite the capacity loss experienced when cycled until 4.8 V, the pyro-LVP/C cathode registers average discharge capacities of 137  $\text{mAh/g}$  at 1280  $\text{mA/g}$  (6.4 C) and 77  $\text{mAh/g}$  at 2000  $\text{mA/g}$  (10 C), as shown in Figures 7(c, d). As the initial set of current densities progressing from 0.05 C to 10 C are repeated sequentially from the 28<sup>th</sup> cycle, the LVP/C cathode still delivers discharge capacities of 140 and 134  $\text{mAh/g}$  at 640 (3.2 C) and 1280  $\text{mA/g}$  (6.4 C) current rates respectively. A hydrothermally prepared Sc-doped LVP ( $\text{Li}_3\text{V}_{1.85}\text{Sc}_{0.15}(\text{PO}_4)_3/\text{C}$ ) cathode was reported to demonstrate capacities of 80  $\text{mAh/g}$  at 5 C rates within a potential window of 3–4.8 V<sup>37</sup>. Other reported hydrothermal routes to one dimensional nanostructures and micro-flakes of LVP yielded capacities of 101 and 164  $\text{mAh/g}$  at 10 and 5 C rates respectively<sup>39</sup>. The registered capacities in the present study are comparable to those reported



for other monoclinic- $\text{Li}_3\text{V}_2(\text{PO}_4)_3$  cathodes cycled until high cut-off potentials of 4.8 V<sup>11,17,18</sup>. The impressive rate capabilities of the prepared LVP/C may be explained on the basis of several reasons. Firstly, the polyol combustion provides spontaneous ultrahigh energies that facilitate the nucleation and growth of amorphous particles. During post-heat treatment, the amorphous LVP undergo phase transition to highly crystalline LVP nanoparticles. The carbonized structures that formed as a result of the polyol combustion may serve as barriers and thus tend to inhibit particle growth. Secondly, the short time durations of post-heat treatment ensures the presence of carbon in the final product. The polyol carbonization also enables carbon painting on particle surfaces which can in turn act as electrical conduits during electrochemical reaction. Thirdly, the presence of a carbon-network appears to favor better particle-connectivity and hence improve the electronic conductivities and contribute to high rate performance. Moreover, the presence of rod-type particles in addition to nano-scaled particles may offer better inter-particle connectivity and thereby contribute to enhanced electrochemical performances<sup>35</sup>. The surface morphology of the as-prepared sample (not shown) clearly indicates the presence of just spherically shaped particles with almost similar particle-sizes in the annealed sample. However, the major difference lies in the fact that annealing produces random growth of rod-type crystals, as presented in Figure 3. Furthermore, the preparation process adopted in the present study is a cost-effective and comparatively faster process than conventional techniques and may lead to the possibilities for large-scale development of cathode materials for high power lithium ion batteries<sup>24</sup>.

In summary, a polyol assisted pyro-synthetic reaction was used to obtain a monoclinic LVP/C cathode with mixed morphologies for lithium batteries. A combined refinement was performed on the XRD and neutron diffraction data to determine the lattice parameter values. The LVP/C cathode revealed morphologies of carbon-coated spherical/rod-type particles by using SEM and TEM studies. The prepared LVP/C cathode demonstrated initial discharge capacities of 131 and 196 Ah/g, equivalent to 100% theoretical capacities of 132 and 197 mAh/g within the potential windows of 3–4.3 and 3–4.8 V that correspond to 2 and 3 Li extractions at current densities of 0.15 and 0.1 C respectively. More importantly, remarkable average specific capacities of 125 and 90 mAh/g at current densities of 1280 and 2000 mA/g respectively were delivered by the LVP cathode within the smaller potential range and may suit high power applications. The impressive rate capabilities of the prepared LVP/C may be attributed to the effective surface carbon-coating on the LVP particles. In addition, the presence of a carbon network also appears to contribute to the impressive electrochemical performance. Moreover, the mixed morphology of nanorods and spherical particles may enhance electrochemical performance. Furthermore, the rapid pyro-synthesis adopted in the present study may offer opportunities not only to realize phosphate-based electrodes for battery applications but also may provide solutions to scale-up the production of prospective energy materials.

## Methods

**Material synthesis.**  $\text{Li}_3\text{V}_2(\text{PO}_4)_3$  powders were obtained by the pyro-synthetic approach using Lithium acetate ( $\text{C}_2\text{H}_3\text{LiO}_2$ ,  $\geq 99\%$  - Aldrich), vanadium acetylacetonate ( $\text{C}_{15}\text{H}_{21}\text{O}_6\text{V}$ , 97% - Aldrich), and phosphoric acid ( $\text{H}_3\text{PO}_4$ ,  $\geq 85\%$  - Daejung) as starting materials. Initially, the starting precursors were dissolved in 80 mL of ethylene glycol ( $\text{C}_2\text{H}_6\text{O}_2$ ,  $\geq 99\%$  - Daejung) in the molar ratio 1.5 : 1 : 1.5 (Li : V : P) at room temperature. After obtaining a homogenous solution, the final solution was uniformly poured onto a hot-plate maintained at 200 °C. The polyol precursor solution was ignited with a torch to induce a self-extinguishable combustion process. Subsequently, the as-prepared powder was annealed at 800 °C for 5 h under argon atmosphere to obtain the LVP/C powders with high crystallinity.

**Neutron and X-ray diffraction studies.** Neutron powder diffraction (NPD) data were collected at room temperature for the prepared sample using a high-resolution powder diffractometer (HRPD) at the Hanaro Center of Korea Atomic Energy Research Institute. The neutron diffraction studies were performed over scattering

angles ranging from 15° to 160° using 1.8367 Å neutrons, with 4 h of collection time per pattern. 5 g of the sample was contained in a vanadium can. Diffraction data were co-refined with X-ray diffraction (XRD) data obtained from a MPD X-ray diffractometer with Cu K $\alpha$  radiation ( $\lambda = 1.5406$  Å) operating at 40 kV and 30 mA within the scanning angle, 2 $\theta$ , ranging between 20 and 100° in steps of 0.02°, using the General Structure Analysis System (GSAS)<sup>40</sup>.

**Electron microscopy (HR-TEM and FE-SEM) analyses.** The particle morphologies and sizes were determined by field emission-scanning electron microscopy (FE-SEM) using an S-4700 model from HITACHI. The High-resolution transmission electron microscopy (HR-TEM) and transmission electron microscopy (TEM) images were recorded using an FEI Tecnai F20 at a 200 kV accelerating voltage.

**Molar stoichiometric and surface area studies.** The stoichiometric molar composition of  $\text{Li}_3\text{V}_2(\text{PO}_4)_3/\text{C}$  was analyzed by inductively coupled plasma atomic emission spectrometer (ICP-AES) using OPIMA 4300 DV from Perkin Elmer. The sample surface area was measured by the Brunauer Emmett and Teller (BET) method using a Micromeritics ASAP2010 (Norcross, GA, USA) instrument.

**Electrochemical characterization.** The electrochemical properties of the  $\text{Li}_3\text{V}_2(\text{PO}_4)_3$  particles were evaluated using lithium metal as the reference electrode. The cathode was fabricated by mixing the active material with 23 wt% carbon (16 wt% carbon black plus the ~ 7 wt% carbon already present in the active material) and polytetrafluoroethylene (PTFE) (7 wt%) was used as a binder. Usually, a loading of 3.5 mg  $\text{cm}^{-2}$  as the active material was used. This mixture was pressed onto a stainless steel mesh and dried under vacuum at 150 °C for 10 h. The cell consisted of a cathode and lithium metal anode separated by glass fiber. The electrolyte used was a propylene carbonate (EC) containing 1 M LiPF<sub>6</sub>.

**In-situ XRD measurements.** The in-situ XRD measurements were performed at beamline 1D KIST-PAL, Pohang Accelerator Laboratory (PAL) using a MAR345-image plate detector operating at 2.5 GeV with a maximum storage current of 200 mA. The X-ray beam was focused by a toroidal mirror and monochromatized to 12.4016 keV (0.9997 Å) by a doublebounce Si (111) monochromator. The Si(111) monochromator and a Si(111) analyzer crystal were used to provide a high-resolution configuration in reciprocal space. The patterns were recorded based on the wavelength value of 0.999 Å. However, the XRD patterns displayed in the present study were plotted after re-calculation of 2 $\theta$  values based on the conventional Cu K $\alpha$  radiation ( $\lambda = 1.5414$  Å). During the preparation of the in-situ cell, the electrode active material mixed with carbon black and PTFE binder (in the ratio mentioned earlier) was cast on stainless steel mesh and assembled in a spectro-electrochemical cell. The cell was cycled to a fully charged/discharged state by a portable potentiostat at constant rate of 0.1 mA/cm<sup>2</sup>. Kapton tape was applied on the apertures of the outer cases of the test cell.

- Whittingham, M. S. Lithium batteries and cathode materials. *Chem. Rev.* **104**, 4271–4302 (2004).
- Padhi, A. K., Nanjundaswamy, K. S. & Goodenough, J. B. Phospho-olivines as positive-electrode materials for rechargeable lithium batteries. *J. Electrochem. Soc.* **144**, 1188–1194 (1997).
- Wu, X. L., Jiang, L. Y., Ca, F. F., Guo, Y. G. & Wan, L. J. LiFePO<sub>4</sub> nanoparticles embedded in a nanoporous carbon matrix: Superior cathode material for electrochemical energy-storage devices. *Adv. Mater.* **21**, 2710–2714 (2009).
- Li, G. H., Azuma, H. & Tohda, M. LiMnPO<sub>4</sub> as the cathode for lithium batteries. *Electrochem. Solid State Lett.* **5**, A135–A137 (2002).
- Huang, H., Yin, S.-C., Kerr, T., Taylor, N. & Nazar, L. F. Nanostructured composites: A high capacity fast rate  $\text{Li}_3\text{V}_2(\text{PO}_4)_3/\text{Carbon}$  cathode for rechargeable lithium batteries. *Adv. Mater.* **14**, 1525–1528 (2002).
- Okada, S. *et al.* Cathode properties of phospho-olivine LiMPO<sub>4</sub> for lithium secondary batteries. *J. Power Sources* **97–98**, 430–432 (2004).
- Padhi, A. K., Nanjundaswamy, K. S., Masquelier, C., Okada, S. & Goodenough, J. B. Effect of structure on the Fe<sup>3+</sup>/Fe<sup>2+</sup> redox couple in iron phosphates. *J. Electrochem. Soc.* **144**, 1609–1613 (1997).
- Nagaura, T. & Tozawa, K. Lithium ion rechargeable battery. *Prog. Batteries Sol. Cells* **9**, 209–217 (1990).
- Jiang, J. & Dahn, J. ARC studies of the thermal stability of three different cathode materials: LiCoO<sub>2</sub>; Li[Ni<sub>0.1</sub>Co<sub>0.8</sub>Mn<sub>0.1</sub>]O<sub>2</sub>; and LiFePO<sub>4</sub>, in LiPF<sub>6</sub> and LiBoB EC/DEC electrolytes. *Electrochem. Commun.* **6**, 39–43 (2004).
- Chang, C. *et al.* Hydrothermal synthesis of carbon-coated lithium vanadium phosphate. *Electrochim. Acta* **54**, 623–627 (2008).
- Liu, H., Gao, P., Fang, J. & Yang, G.  $\text{Li}_3\text{V}_2(\text{PO}_4)_3/\text{graphene}$  nanocomposites as cathode material for lithium ion batteries. *Chem. Commun.* **47**, 9110–9112 (2011).
- Ren, M. M., Zhou, Z., Gao, X. P., Peng, W. X. & Wei, J. P. Core-shell  $\text{Li}_3\text{V}_2(\text{PO}_4)_3/\text{C}$  composites as cathode materials for lithium-ion batteries. *J. Phys. Chem. C* **112**, 5689–5693 (2008).
- Wang, C., Liu, H. & Yang, W. An integrated core-shell structured  $\text{Li}_3\text{V}_2(\text{PO}_4)_3/\text{C}$  cathode material of LIBs prepared by a momentary freeze-drying method. *J. Mater. Chem.* **22**, 5281–5285 (2012).
- Kim, D. H. & Kim, J. Synthesis of LiFePO<sub>4</sub> nanoparticles in polyol medium and their electrochemical properties. *Electrochem. Solid-State Lett.* **9**, A439–A442 (2006).





15. Pan, A. *et al.* Nano-structured  $\text{Li}_3\text{V}_2(\text{PO}_4)_3/\text{carbon}$  composite for high-rate lithium-ion batteries. *Electrochem. Commun.* **12**, 1674–1677 (2010).
16. Wang, L., Zhou, X. & Gou, Y. Synthesis and performance of carbon-coated  $\text{Li}_3\text{V}_2(\text{PO}_4)_3$  cathode materials by a low temperature solid-state reaction. *J. Power Sources* **195**, 2844–2850 (2010).
17. Qiao, Y. Q. *et al.* Effects of synthetic route on structure and electrochemical performance of  $\text{Li}_3\text{V}_2(\text{PO}_4)_3/\text{C}$  cathode materials. *Electrochim. Acta* **56**, 4139–4145 (2011).
18. Fu, P., Zhao, Y., Dong, Y., An, X. & Shen, G. Synthesis of  $\text{Li}_3\text{V}_2(\text{PO}_4)_3$  with high performance by optimized solid-state synthesis routine. *J. Power Sources* **162**, 651–657 (2006).
19. Li, Y., Liu, X. & Yan, J. Study on synthesis routes and their influences on chemical and electrochemical performances of  $\text{Li}_3\text{V}_2(\text{PO}_4)_3/\text{carbon}$ . *Electrochim. Acta* **53**, 474–479 (2007).
20. Patoux, S., Wurm, C., Morcrette, M., Rousse, G. & Masquelier, C. A comparative structural and electrochemical study of monoclinic  $\text{Li}_3\text{Fe}_2(\text{PO}_4)_3$  and  $\text{Li}_3\text{V}_2(\text{PO}_4)_3$ . *J. Power Sources* **119–121**, 278–284 (2003).
21. Zhou, X., Liu, Y. & Guo, Y. Effect of reduction agent on the performance of  $\text{Li}_3\text{V}_2(\text{PO}_4)_3/\text{C}$  positive material by one-step solid-state reaction. *Electrochim. Acta* **54**, 2253–2258 (2009).
22. Kang, J. *et al.* High rate performance of a  $\text{Na}_3\text{V}_2(\text{PO}_4)_3/\text{C}$  cathode prepared by pyro-synthesis for sodium-ion batteries. *J. Mater. Chem.* **22**, 20857–20860 (2012).
23. Wang, L., Zhang, L.-C., Lieberwirth, I., Xu, H. W. & Chen, C. H. A  $\text{Li}_3\text{V}_2(\text{PO}_4)_3/\text{C}$  thin film with high rate capability as a cathode material for lithium-ion batteries. *Electrochem. Commun.* **12**, 52–55 (2010).
24. Gim, J. *et al.* Pyro-synthesis of functional nanocrystals. *Sci Rep.* **2**, 946 (2012).
25. Gao, C., Liu, H., Liu, G., Zhang, J. & Wang, W. High-rate performance of  $\text{xLiFePO}_4 \cdot \text{yLi}_3\text{V}_2(\text{PO}_4)_3/\text{C}$  composite cathode materials. *Mater. Sci. Eng. B* **178**, 272–276 (2013).
26. Nathiya, K., Bhuvaneshwari, D., Gangulibabu & Kalaiselvi, N. Combustion synthesized nanocrystalline  $\text{Li}_3\text{V}_2(\text{PO}_4)_3/\text{C}$  cathode for lithium-ion batteries. *Mater. Res. Bull.* **47**, 4300–4304 (2012).
27. Kalidas, N., Nallathamby, K. & Minakshi, M. Oxalic Dihydrate Assisted novel combustion synthesized  $\text{Li}_3\text{V}_2(\text{PO}_4)_3$  and  $\text{LiVP}_2\text{O}_7$  compounds for rechargeable lithium batteries. *ECS Trans.* **50**, 79–88 (2013).
28. Laoutid, F., Bonnaud, L., Alexandre, M., Lopez-Cuesta, J. M. & Dubois, Ph. New prospects in flame retardant polymer materials: From fundamentals to nanocomposites. *Mat. Sci. Eng. R* **63**, 100–125 (2009).
29. Yin, S.-C., Grondy, H., Strobel, P., Anne, M. & Nazar, L. F. Electrochemical property: structure relationships in monoclinic  $\text{Li}_{3-\gamma}\text{V}_2(\text{PO}_4)_3$ . *J. Am. Chem. Soc.* **125**, 10402–10411 (2003).
30. Liu, H. *et al.* Kinetics of conventional carbon coated-  $\text{Li}_3\text{V}_2(\text{PO}_4)_3$  and nanocomposite  $\text{Li}_3\text{V}_2(\text{PO}_4)_3/\text{graphene}$  as cathode materials for lithium ion batteries. *J. Mater. Chem.* **22**, 11039–11047 (2012).
31. Kuo, H. T. *et al.* Structural Transformation of  $\text{LiVOPO}_4$  to  $\text{Li}_3\text{V}_2(\text{PO}_4)_3$  with enhanced Capacity. *J. Phys. Chem. B* **112**, 11250–11257 (2008).
32. Yang, G., Liu, H., Ji, H., Chen, Z. & Jiang, X. Temperature-controlled microwave solid-state synthesis of  $\text{Li}_3\text{V}_2(\text{PO}_4)_3$  as cathode materials for lithium batteries. *J. Power Sources* **195**, 5374–5378 (2010).
33. Barker, J., Saidi, M. Y. & Swoyer, J. L. A carbothermal reduction method for the preparation of electroactive materials for lithium ion applications. *J. Electrochem. Soc.* **150**, A684–A688 (2003).
34. Wang, J. *et al.* Comparative investigations of  $\text{LiVPO}_4\text{F}/\text{C}$  and  $\text{Li}_3\text{V}_2(\text{PO}_4)_3/\text{C}$  synthesized in similar soft chemical route. *J. Solid State Electrochem.* **17**, 1–8 (2013).
35. Lim, J., Mathew, V., Kim, K., Moon, J. & Kim, J. One-pot synthesis of multi-morphous  $\text{LiFePO}_4$  nanoparticles in polyol medium. *J. Electrochem. Soc.* **158**, A736–A740 (2011).
36. Rui, X. H., Lia, C., Liu, J., Cheng, T. & Chen, C. H. The  $\text{Li}_3\text{V}_2(\text{PO}_4)_3/\text{C}$  composites with high-rate capability prepared by a maltose-based sol–gel route. *Electrochim. Acta.* **55**, 6761–6767 (2010).
37. Sun, C., Rajasekhara, S., Dong, Y. & Goodenough, J. B. Hydrothermal synthesis and electrochemical properties of  $\text{Li}_3\text{V}_2(\text{PO}_4)_3/\text{C}$ -based composites for lithium-ion batteries. *ACS Appl. Mater. Interfaces* **3**, 3772–3776 (2011).
38. Yoon, J. *et al.* Study on structure and electrochemical properties of carbon-coated monoclinic  $\text{Li}_3\text{V}_2(\text{PO}_4)_3$  using synchrotron based in situ X-ray diffraction and absorption. *J. Alloys Cds.* **569**, 76–81 (2013).
39. Liu, H., Cheng, C., Huang, X. & Li, J. Hydrothermal synthesis and rate capacity studies of  $\text{Li}_3\text{V}_2(\text{PO}_4)_3$  nanorods as cathode material for lithium-ion batteries. *Electrochim. Acta* **55**, 8461–8465 (2010).
40. Larson, A. C. & Von Dreele, R. B. General Structure Analysis System (GSAS). Los Alamos National Laboratory Report LAUR 86–748 (1994), <http://www.ccp14.ac.uk/solution/gsas/> (accessed on 15/01/2014).

## Acknowledgments

This work was supported by Industrial Strategic Technology Development Program (10045401, Development of high-voltage multi-transition metal phosphate cathode material) funded by the Ministry of Trade, Industry & Energy (MOTIE, Korea) and also by MSIP (Ministry of Science, ICT & Future Planning), Korea, under the C-ITRC (Convergence Information Technology Research Center) support program (NIPA-2013-H0301-13-1009) supervised by the NIPA (National IT Industry Promotion Agency).

## Author contributions

J.K. directed the research. Jw.K., V.M., J.G., S.K. & J.S. performed the experiments and characterizations. Jw.K. & V.M. wrote the manuscript. Jw.K., J.G. & V.M. prepared the Figures. W.B.I. performed the neutron diffraction studies and contributed to editing the corresponding portion in the manuscript. J.H. & J.Y.L. contributed to TEM analysis. All the authors contributed toward the technical discussions of results and reviewed the paper.

## Additional information

Supplementary information accompanies this paper at <http://www.nature.com/scientificreports>

Competing financial interests: The authors declare no competing financial interests.

How to cite this article: Kang, J.W. *et al.* Pyro-synthesis of a high rate nano- $\text{Li}_3\text{V}_2(\text{PO}_4)_3/\text{C}$  cathode with mixed morphology for advanced Li-ion batteries. *Sci. Rep.* **4**, 4047; DOI:10.1038/srep04047 (2014).



This work is licensed under a Creative Commons Attribution-NonCommercial-NoDerivs 3.0 Unported license. To view a copy of this license, visit <http://creativecommons.org/licenses/by-nc-nd/3.0>